

RSC Advances

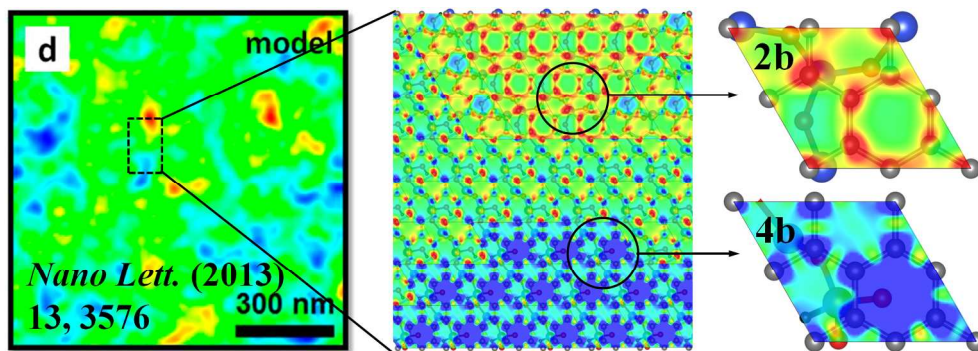


This is an *Accepted Manuscript*, which has been through the Royal Society of Chemistry peer review process and has been accepted for publication.

Accepted Manuscripts are published online shortly after acceptance, before technical editing, formatting and proof reading. Using this free service, authors can make their results available to the community, in citable form, before we publish the edited article. This *Accepted Manuscript* will be replaced by the edited, formatted and paginated article as soon as this is available.

You can find more information about *Accepted Manuscripts* in the [Information for Authors](#).

Please note that technical editing may introduce minor changes to the text and/or graphics, which may alter content. The journal's standard [Terms & Conditions](#) and the [Ethical guidelines](#) still apply. In no event shall the Royal Society of Chemistry be held responsible for any errors or omissions in this *Accepted Manuscript* or any consequences arising from the use of any information it contains.



graphical abstract
191x67mm (300 x 300 DPI)

Cite this: DOI: 10.1039/c0xx00000x

www.rsc.org/xxxxxx

ARTICLE TYPE

Charge inhomogeneity of graphene on SiO₂: Dispersion-corrected density functional theory study on the effect of reactive surface sites

Jinhee Lee,^a Nodo Lee,^a Yves Lansac^{*a,b} and Yun Hee Jang^{*a}

Received (in XXX, XXX) Xth XXXXXXXXX 20XX, Accepted Xth XXXXXXXXX 20XX

DOI: 10.1039/b000000x

Graphene is a promising high-mobility material, but the mobility of graphenes supported on a substrate is far from the theoretical limit. The degradation of remarkable electronic properties is often attributed to a spatial charge inhomogeneity, so-called *charge puddle*, present in supported graphenes. Since the most widely used substrate for electronic devices, amorphous SiO₂, tends to expose various types of surface species, we investigate how a variety of surface species present on amorphous SiO₂ substrates would affect the electronic structure of graphenes on them. Four representative surface species (saturated and unsaturated) are constructed on pristine SiO₂ (001) surfaces, and a dispersion-corrected spin-polarized density functional theory calculation is carried out on a graphene sheet bound on each of them. The calculation shows that, among the four model species, the unsaturated model with exposed oxygen dangling bonds is the only surface species which can bind graphene rather strongly. Only this one accepts a significant amount of electrons from graphene, leading to a non-negligible amount of *p*-doping and band-gap opening of graphene. Such reactive surface species present in a mixture with inert ones could be one likely origin of the *charge puddle* observed in supported graphenes. A thermal annealing or passivation of oxygen dangling bonds on SiO₂ would reduce charge puddle in supported graphenes.

1 Introduction

Graphene is a two-dimensional sheet of carbon atoms packed into a honeycomb lattice, which constitutes a single-atomic-layer building block of graphite.^{1,2} It has great potential to use in electronic devices, owing to high mobilities of its charge carriers, both electrons and holes.^{1,3-5} In most devices, however, graphene is supported by a silicon dioxide (SiO₂) dielectric layer, and the mobility measured on supported graphenes is far from the theoretical limit and highly vulnerable to external conditions.^{3,6} The degradation of remarkable electronic properties of graphene is often attributed to a spatial charge inhomogeneity observed in supported graphenes: some areas in a graphene sheet display excess of electrons and some other areas exhibit excess of holes, inducing extra electron scattering and reduced mobility.⁷⁻¹⁰ The origin of the so-called *electron-hole puddle* or *charge puddle*^{2,7,11} is not clear yet.¹² It could come from corrugations or ripples of graphene, either intrinsic (found in free-standing graphenes)¹³⁻¹⁵ or extrinsic (conforming to the corrugation of the underlying SiO₂ substrate),¹⁶⁻¹⁸ and also from charged impurities (H₂O or other unknown moieties which survive vacuum annealing)^{22,23} present either between graphene and SiO₂ or on top of graphene.^{11,19-23} A recent Kelvin probe force microscopy study²¹ has reported that a high degree of potential disorder and charge inhomogeneity of amorphous SiO₂ substrate itself (compared to h-BN) is related to the mobility reduction in graphene on it. Electron beam exposure (often employed in graphene fabrication) increases the charge density fluctuation by producing a large amount of metastable charge traps on SiO₂, which is reversed by thermal annealing.²¹

We therefore speculate that the presence of unsaturated reactive surface species produced on the underlying SiO₂ substrate during device fabrication could be responsible for the charge puddle of supported graphenes. We therefore investigate the effect of a variety of saturated and unsaturated SiO₂ surface species on the electronic structure of graphene, by performing density functional theory (DFT) calculations on several model surfaces.

The most stable polymorph of SiO₂ is α -quartz and its most stable surface is (001).^{24,25} The pristine (001) surface exposes unsaturated dangling bonds ($\bullet\text{SiO}\bullet$; **0** in Fig. 1), which can be saturated by dissociative adsorption of water on both sides of the dangling bond to form a pair of geminal silanols (HOSiOH; **1** in Fig. 1).^{24,26} At temperatures above 300 K, the saturation can also be achieved by a surface reconstruction connecting adjacent dangling bonds (SiOSi; **2** in Fig. 1).^{24,25,27} These surface models (*hydrated* or *fully-hydroxylated 1* and *reconstructed 2*) have been used in DFT calculations on graphenes supported by SiO₂.²⁸⁻³⁴ However, we expect that, in addition to the saturated species, a significant amount of unsaturated surface species with silicon ($\text{Si}\bullet$) and oxygen ($\text{O}\bullet$) dangling bonds should exist on amorphous SiO₂ substrates used in most electronic devices, as a result of laser/ion radiation or plasma treatment in the course of device fabrication. We model these unsaturated sites by two types of *partially-hydrogenated* intermediates of H₂ passivation of the pristine (001) surface **0**,³⁵ where a hydrogen atom has been added either to the oxygen dangling bond ($\bullet\text{SiO}\bullet + \text{H}\bullet \rightarrow \bullet\text{SiOH}$; **3** in Fig. 1) or to the silicon dangling bond ($\text{H}\bullet + \bullet\text{SiO}\bullet \rightarrow \text{HSiO}\bullet$; **4** in Fig. 1), leaving a silicon ($\text{Si}\bullet$) and oxygen ($\text{O}\bullet$) dangling bond, respectively. The interaction between a graphene sheet and each

of the four representative (two stable and two reactive) SiO₂ surfaces **1–4** and the resulted charge transfer between them are calculated and related to the substrate-induced spatial charge inhomogeneity, that is, charge puddle of graphene.

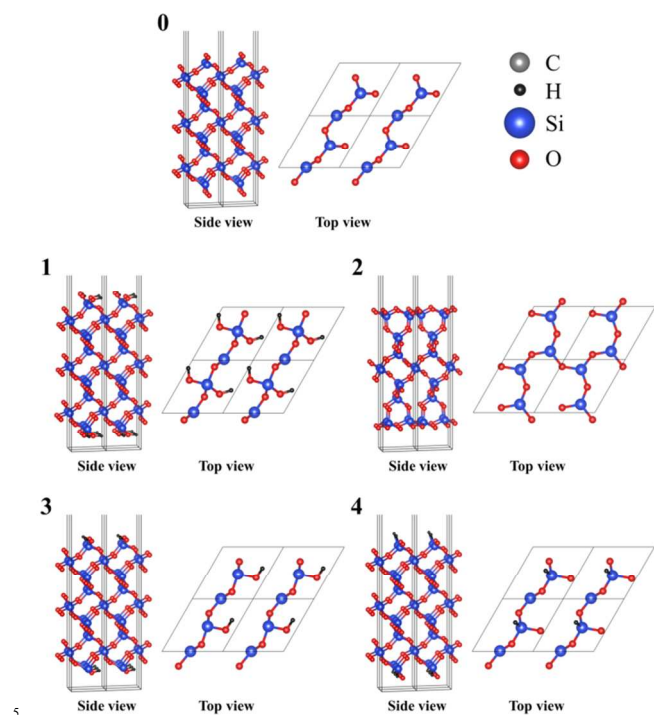


Fig. 1 Side (left) and top (right) views on α -quartz SiO₂ (001) surface with \bullet SiO \bullet dangling bonds (**0**; top) and on four (two saturated and two unsaturated) surfaces built from it: hydrated **1** (HOSiOH), reconstructed **2** (SiOSi) and partially-hydrogenated **3** (with silicon dangling bonds \bullet SiOH) and **4** (with oxygen dangling bonds HSiO \bullet). Color code: black (H), red (O), blue (Si), and black solid line (unit-cell lattice).

2 Calculation Details

2.1 Model

Periodic slab models are used to represent the four SiO₂ (001) surfaces **1–4** (Fig. 1) and their interfaces with a graphene sheet **1a–4b** (Fig. 2). On the basis of the convergence test of Goumans and coworkers,²⁴ we represent the surfaces **1–4** by three-unit-cell-high slabs cut from a hexagonal α -quartz crystal ($a = 4.916$ Å, $c = 5.405$ Å).³⁶ The lateral lattice parameters of these slab models (4.916 Å) are scaled up by 0.2% to match those of graphite and graphene (4.928 Å).³⁷ A vacuum slab of ~ 19 Å (which is chosen from a convergence test; not shown here) is inserted between the slabs in vertically adjacent unit cells in order to avoid fictitious interactions between the images of slabs. These slab models **1–4** are submitted to an optimization of atomic positions at the lattice parameters fixed at 4.928 Å and 35.256 Å.

Right on top of the topmost oxygen atom of the optimized slab models **1–4**, either a carbon atom (*on-top* configuration **a**) or the center of a hexagon of carbon atoms (*hollow* configuration **b**) of an ideally-flat single-layer graphene sheet is placed to build the eight different periodic slab models of the graphene/SiO₂ interface (**1a–4b**; Fig. 2). A vacuum slab of ~ 15 Å is inserted between the composite slabs in vertically adjacent unit cells. These slab models **1a–4b** are submitted to an optimization of atomic positions at the lattice parameters fixed at 4.928 Å and 35.256 Å.

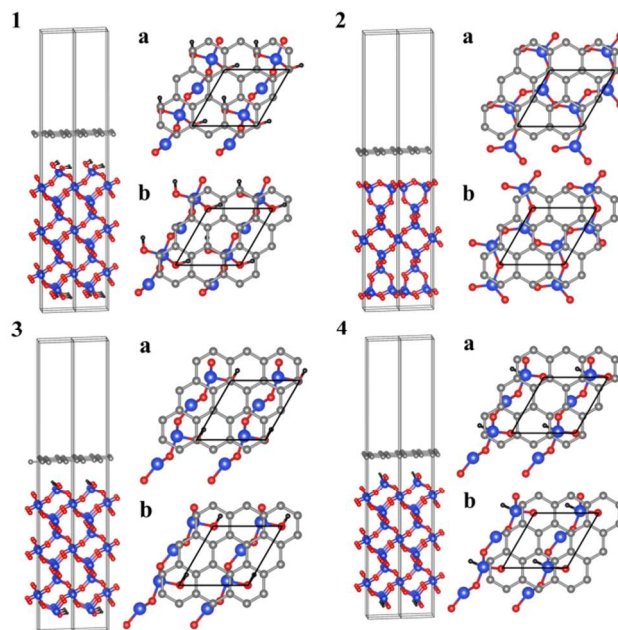


Fig. 2 Side (left) and top (right) views on the optimized structures of eight graphene/SiO₂ interface models, where a graphene sheet is adsorbed on four SiO₂ surface models [HOSiOH (**1**), SiOSi (**2**), \bullet SiOH (**3**), and HSiO \bullet (**4**)] in two configurations (*on-top* **a** and *hollow* **b**). Only the topmost SiO₂ layer is shown in the top views (right) for clarity. Color code: black (H), grey (C), red (O), blue (Si), and black solid line (unit-cell lattice).

2.2 Calculation Method

Periodic DFT calculations are carried out using the VASP code.³⁸ A dispersion correction scheme of Grimme^{39,40} is used in conjunction with the PBE functional^{41,42} to describe correctly the interaction between graphene and SiO₂ surfaces, as done by Fan and coworkers.³⁴ This PBE-D functional is known to describe the adsorption of organic molecules quite well (with a certain degree of overestimation).^{43,44} The core electrons of each atom are replaced by the projector-augmented-wave pseudopotentials,^{45,46} and the outer valence electrons (4 electrons in Si 3s/3p, 6 in O 2s/2p, 4 in C 2s/2p, and 1 in H 1s) are described by a set of plane waves with kinetic energies up to 600 eV. Spin-polarized calculations are carried out for the unsaturated surfaces **3–4** and their composites with graphene **3a–4b**. For saturated surfaces **1–2** and their composites with graphene **1a–2b**, both spin-unpolarized and spin-polarized calculations give the same results. On the basis of a convergence test on the bulk SiO₂ α -quartz crystal (not shown), the Brillouin-zone integration is performed on a set of k-points generated by a $7 \times 7 \times 1$ Γ -point-centered Monkhorst-Pack mesh⁴⁷ with a Gaussian smearing of 0.2 eV. The convergence criterion for the electronic self-consistent-field cycle is 1×10^{-5} eV. For geometry optimization, the atomic coordinates are fully relaxed with a conjugate gradient method until the energy change is less than 1×10^{-4} eV. At the final geometry, the band structure, DOS, and a series of partial DOS projected onto each group of atoms (PDOS) are analyzed with a $21 \times 21 \times 1$ Monkhorst-Pack k-point mesh and a tetrahedron method.⁴⁸ The number of valence electrons carried by each atom (and thus the atomic charge) is estimated by the Bader analysis, which partitions a charge density grid into Bader volumes whose dividing surfaces, so-called zero-flux surfaces, lie in the bonding regions between atoms.^{49–51} The model structures and charge densities are visualized by VESTA.⁵²

3 Results and Discussion

3.1 Stabilities of SiO₂ Surfaces 1–4

The relative stabilities of the surface species **1–4** (Fig. 1) are measured by a surface energy (E_{surf} ; Table 1) defined as^{24,53}

$$E_{\text{surf}} = (2A)^{-1} \times [E(\text{slab}) - E(\text{bulk}) - E(\text{ads})]. \quad (1)$$

Less positive numbers represent more stable surfaces. A is the surface area of the unit cell ($0.2103 \text{ nm}^2 = 4.928 \text{ \AA} \times 4.928 \text{ \AA} \times \sin 60^\circ$), $E(\text{slab})$ is the total energy of each SiO₂ slab (**1–4**; Fig. 1), and $E(\text{bulk})$ is the total energy of the bulk α -quartz SiO₂ crystal whose unit cell contains the same number of atoms as the stoichiometric slab **2** (nine formula units of SiO₂). $E(\text{ads})$ is zero for the stoichiometric slab **2**. For non-stoichiometric surfaces **1** and **3–4**, $E(\text{ads})$ is the total energy (at the most stable phase) of molecules added to both sides of **2** to create **1** [$2E(\text{H}_2\text{O}(l)) = 2E(\text{H}_2\text{O}(g)) - 2\Delta E_{\text{vap}}(\text{H}_2\text{O})$] or **3–4** [$E(\text{H}_2(g))$]. The total energy of a gas-phase molecule, $E(\text{H}_2\text{O}(g))$ or $E(\text{H}_2(g))$, is calculated in a cubic cell of a size of 10 \AA . The energy of vaporization ΔE_{vap} is given from the experimental enthalpy of vaporization at room temperature⁵⁴ with the ideal gas approximation [$\Delta H_{\text{vap}} - P\Delta V_{\text{vap}} \approx \Delta H_{\text{vap}} - RT = 43.990 - 2.479 = 41.511 \text{ kJ/mol} = 0.43022 \text{ eV}$].

Table 1 SiO₂: surface energy (E_{surf}).^a

(Fig. 1) Surface model	PBE			PBE-D		
	$E(\text{slab})$ eV	$E(\text{ads})$ eV	E_{surf} eV/nm ²	$E(\text{slab})$ eV	$E(\text{ads})$ eV	E_{surf} eV/nm ²
1	-242.3 ^b	-29.3 ^d	0.7 ^f	-245.2 ^b	-29.3 ^d	0.9 ^f
2	-212.0 ^b	0.0	3.1 ^g	-214.5 ^b	0.0	4.2 ^g
3	-214.7 ^c	-6.8 ^e	12.8	-217.3 ^c	-6.8 ^e	13.6
4	-212.1 ^c	-6.8 ^e	18.8	-214.7 ^c	-6.8 ^e	19.7

^a Eq. (1), $E(\text{bulk}) = -213.3$ (PBE), -216.3 (PBE-D) eV; $2A = 0.4206 \text{ nm}^2$.

^b From spin-unpolarized calculations. ^c From spin-polarized calculations.

^d $2E(\text{H}_2\text{O}(l))$ at 298 K = $2[E(\text{H}_2\text{O}(g)) - \Delta E_{\text{vap}}(\text{H}_2\text{O})] = 2[-14.22 - 0.43]$.

^e $E(\text{H}_2(g))$. ^f exp. 0.719 – 1.25 eV/nm^2 . ^g other calc. 2.3 – 5 eV/nm^2 .

The PBE-D values of E_{surf} are higher than the PBE values by ~25% in the case of **1–2** and by ~5% in the case of **3–4**, showing a significant effect of the dispersion correction on the description of weak interaction. Both PBE and PBE-D values, however, show that the model **1** (HOSiOH) is the most stable form of the SiO₂ (001) surface, followed by **2** (SiOSi), **3** (\bullet SiOH), and **4** (HSiO \bullet). For the stable surfaces **1–2**, both PBE and PBE-D values (0.7 – 4.2 eV/nm^2) are comparable with various literature values from experiments (0.719 – $1.25 \text{ eV/nm}^2 = 115$ – 200 mJ/m^2),^{26,55,56} from previous DFT calculations (0.94 – $1.3 \text{ eV/nm}^2 = 150$ – 200 mJ/m^2 for **1**; 2.3 – $3.1 \text{ eV/nm}^2 = 360$ – 490 mJ/m^2 for **2**),²⁴ from classical molecular dynamics simulations ($1.3 \text{ eV/nm}^2 = 0.5 \times 430 \text{ mJ/m}^2$ for **1**; the original literature value is divided by two due to the difference in the definition of the surface energy),⁵³ and from ab initio molecular dynamics simulations (5 eV/nm^2 for **2**).⁵⁷

For the unsaturated surfaces **3–4**, both PBE and PBE-D values of E_{surf} (12.8 – 19.7 eV/nm^2 or 2.7 – 4.1 eV per unit cell which contains one dangling bond) are indeed higher than the values for the saturated surfaces **1–2** (0.7 – 4.2 eV/nm^2 or 0.14 – 0.89 eV per unit cell). The difference in the stability between **1–2** and **3–4** is less than 4 eV per dangling bond, which is lower than the energy (10^1 – 10^2 eV) provided by incoming particles or radiation in typical etching and sputtering processes.^{58,59} We therefore expect that a significant amount of reactive surface species such as **3–4** should be present in typical graphene devices.

3.2 Stability of Graphene on SiO₂ Surfaces 1a–4b

The stability of graphene on SiO₂ surface in the composite **1a–4b** (Fig. 2) is measured by the binding energy (E_b) defined as

$$E_b = A^{-1} \times [E(\text{G}) + E(\text{SiO}_2) - E(\text{G/SiO}_2)]. \quad (2)$$

$E(\text{G/SiO}_2)$ is the total energy of the graphene/SiO₂ composite **1a–4b**, $E(\text{G})$ is the total energy of an ideally-flat free-standing single-layer graphene, and $E(\text{SiO}_2)$, which is the same as $E(\text{slab})$ of Eq. 1, is the total energy of the bare SiO₂ slab **1–4** (Fig. 1). The binding energy E_b should be sufficiently positive ($E_b > 0$) for a stable binding. We first obtain binding energy curves of **1a–4b** by performing a series of geometry optimization with the graphene constrained at a given height d from the topmost oxygen atoms of each SiO₂ surface **1–4** for each binding configuration **a–b** (Fig. 3). At the minimum-energy height from each SiO₂ surface (that is, at the bottom of each binding energy curve), the constraint is removed and the geometry is fully optimized. The fully optimized geometries of **1a–4b** are shown in Fig. 2, and their equilibrium heights d_e and binding energies E_b are listed in Table 2.

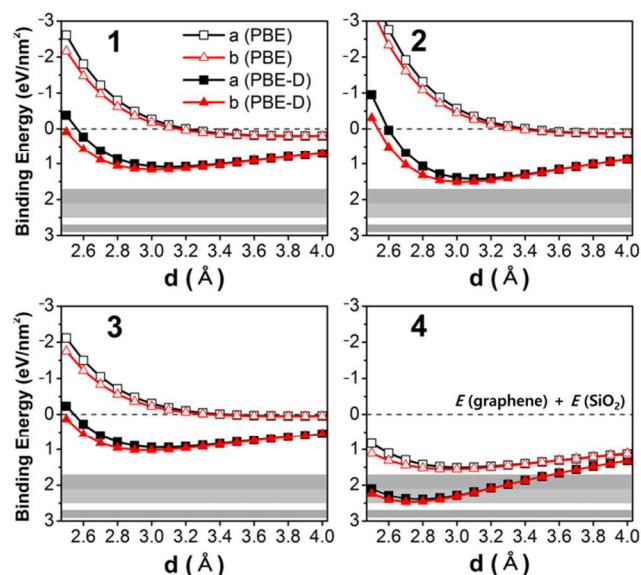


Fig. 3 Binding energy curves for a graphene sheet on SiO₂ surface **1–4** in configuration **a–b** at various heights d from the topmost oxygen atoms of the SiO₂ surface. The horizontal dashed line indicates the reference energy to estimate the binding energy, which is the sum of the total energies of a flat free-standing graphene sheet and of each bare SiO₂ surface **1–4**. The horizontal grey bands indicate a range of experimental binding energies. The PBE and PBE-D values are given together by open marks and filled marks, respectively, to show the effect of the dispersion correction on the description of weak interaction.

Table 2 Graphene/SiO₂: equilibrium distance^a and binding energy.^b

Surface	Site	PBE		PBE-D	
		d_e (Å)	E_b	d_e (Å)	E_b
1	a	3.90	0.2 (0.5)	3.13	1.1 (2.8)
	b	3.90	0.2 (0.5)	3.03	1.2 (3.0)
2	a	4.00	0.1 (0.3)	3.10	1.4 (3.6)
	b	4.00	0.1 (0.3)	2.98	1.5 (3.9)
3	a	3.90	0.05 (0.1)	3.10	1.0 (2.5)
	b	3.80	0.05 (0.1)	3.01	1.1 (2.7)
4	a	2.93	1.5 (3.8)	2.75	2.4 (6.1)
	b	2.86	1.5 (3.9)	2.70	2.5 (6.2)

^a Equilibrium height d_e of graphene from the topmost O atom of SiO₂.

^b eV/nm² (and kJ/mol per C atom in parentheses).

The black and red curves in each graph of Fig. 3 essentially overlap each other. The binding configuration, **a** (black) or **b** (red), of graphene on SiO₂ has a negligible effect. Since the hollow-site binding (**b**; red) is slightly more stable than the on-top-site binding (**a**; black), the following discussions focus on the hollow-site binding **b** (red).

Experimental binding energies are indicated as horizontal grey bands in Fig. 3: 2.8±0.1 eV/nm² (0.45±0.02 J/m²) and 1.9±0.2 eV/nm² (0.31±0.03 J/m²) for single-layer and multilayer graphene, respectively, from a *blister* test on SiO₂ substrates patterned with microcavities,⁶⁰ 2.1 eV/nm² (0.33 J/m²) from an atomic force microscopy study on multiwall carbon nanotubes collapsed onto SiO₂/Si substrates,⁵⁵ and 1.72–2.5 eV/nm² (0.275–0.4 J/m²) from a combination of the surface energies of SiO₂ and of graphite.^{55,61}

In all the graphs of Fig. 3, the PBE-D (filled-mark) curves are positioned much lower and closer to the grey bands than the PBE (open-mark) curves, showing a significant effect of the dispersion correction. With PBE, binding of graphene is not clear at all ($E_b = 0.05\text{--}0.2$ eV/nm² = 0.1–0.5 kJ/mol per C atom at ~4 Å) on the surfaces except **4**, where a clear binding ($E_b = 1.5$ eV/nm² = 3.9 kJ/mol per C atom) is detected at a height d_e of 2.9 Å. On the other hand, with PBE-D, the binding of graphene is clear on all the surfaces **1–4** ($E_b = 1.1\text{--}2.5$ eV/nm² = 2.7–6.2 kJ/mol per C atom) at equilibrium heights d_e of 2.7–3.0 Å. As expected, the PBE-D functional appears more appropriate than PBE to describe the weak interaction between graphene and SiO₂, and thus the following discussions focus on the PBE-D results (filled marks).

It is still intriguing, however, to notice that the PBE-D binding energies (filled marks) on most abundant surfaces **1–2** (1.1–1.5 eV/nm²) still significantly underestimate the experiments (grey bands; 1.7–2.9 eV/nm²). This is surprising because the PBE-D functional is known to overestimate, not underestimate, binding energies.^{43,44} Other shortcomings of our calculations such as the uncorrected basis set superposition errors and the assumption of perfect contacts between ideally-flat graphenes and SiO₂ surfaces would also overestimate, not underestimate, the binding energies. A likely explanation for this would be that the SiO₂ surfaces employed in experiments do not correspond purely to the stable surface models **1–2** but in fact expose a fair amount of reactive surface species such as **3–4**. Indeed the PBE-D value on the surface model **4** (2.5 eV/nm²) is in the best agreement with the experiments (1.7–2.9 eV/nm²). In fact, a creation of dangling bonds on SiO₂ surfaces by using O₂ plasma has been employed to provide a *fixing layer* for strong binding of graphene.⁶²

Since we assume that less stable surfaces exposing reactive surface species would show stronger binding of graphene, it is surprising to find that one of our reactive surfaces **3** ($E_{\text{surf}} = 13.6$ eV/nm²) shows a binding energy E_b of 1.1 eV/nm², which is similar to 1.2 eV/nm² of the most stable surface model **1** ($E_{\text{surf}} = 0.9$ eV/nm²). This should be because the silicon dangling bond (•Si) of **3** is located 1 Å below the hydroxyl (OH) group and does not participate in the interaction with graphene.

Table 3 Graphene/SiO₂: electronic structure at PBE-D geometries.

Model	E_{surf} eV/nm ²	d_e Å	E_b eV/nm ² (kJ/mol/C)	Δq e /C	E_g meV
1b	0.9	3.03	1.2 (3.0)	0.0006	10
2b	4.2	3.10	1.5 (3.9)	0.0016	5
3b	13.6	3.01	1.1 (2.7)	-0.0008	17 (12) ^a
4b	19.7	2.70	2.5 (6.2)	0.0295	24 (24) ^a

^aBand gaps of spin-up (spin-down) components

3.3 Electronic Structure of Graphene/SiO₂

Charge Transfer. Charge density difference maps of **1b–4b** before and after the binding of graphene to **1–4** are defined as

$$\Delta\rho(x, y) = \rho_G(x, y) + \rho_{\text{SiO}_2}(x, y) - \rho_{\text{G/SiO}_2}(x, y), \quad (3)$$

and calculated at a plane at 0.3 Å below the graphene. They are collected into one map (Fig. 4) for a schematic representation of the charge density fluctuation in graphene induced by a variety of surface states (blue for *p*-doping and excess of holes; red for *n*-doping and excess of electrons). Only for **4b** we see a clear development of electron depletion localized on top of the oxygen dangle bond (O•) due to its electronegative nature. Indeed, when O₂ plasma was used to provide a fixing layer for strong binding of graphene by creating dangling bonds on SiO₂, a graphene transistor fabricated on it showed a dominant hole conduction but no electron conduction.⁶² If the graphene layer were perfect with no defect in it, the electron depletion would not be confined in **4b** as much as in Fig. 4. However, in a typical graphene layer which tends to have a large amount of grain boundaries and crack-type line defects, the excess holes produced by oxygen dangling bonds (O•) as in **4b** would be confined within grain boundaries surrounding them and localized in small patchwork-type areas, producing an inhomogeneous charge distribution. We thus propose that a combination of the presence of grain boundaries in graphene and the presence of reactive surface species (O• as in **4b**) in a mixture of various surface species (mostly inert as in **1b–3b**) on SiO₂ could be one likely origin of the charge puddle observed in supported graphenes, partly supporting a previous proposition by Kang and coworkers.²⁸

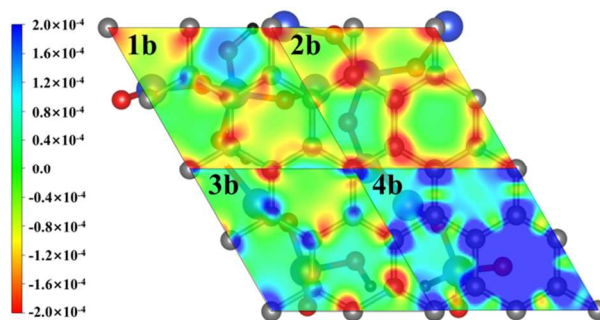


Fig. 4 Charge density fluctuation in a supported graphene schematically represented by collecting the charge density difference maps of **1b–4b** obtained at a plane 0.3 Å below the graphene. The unit of the isovalue is e/Å³. Blue and red regions represent excess of holes and electrons, respectively, in graphene induced by the adsorption on the surfaces **1–4**.

The amount of graphene-to-SiO₂ electron transfer (Δq ; Table 3) is defined as $\Delta q = N_0(\text{C}) - N(\text{C})$, where $N_0(\text{C})$ and $N(\text{C})$ are the numbers of valence electrons of graphene before and after binding on SiO₂ surface, which are estimated from the Bader analysis.^{49–51} As expected from Fig. 4, weakly bound graphenes **1b–3b** lose essentially no charge to SiO₂ ($|\Delta q| \sim 0.001$ |e| per C atom, which corresponds to a doping concentration of $\sim 10^{12}$ cm⁻²). Only the strongly bound graphene **4b** loses a noticeable amount of electrons to SiO₂ to produce a positively-charged (*p*-doped) graphene: $\Delta q \sim 0.03$ |e| per C atom, 0.24 |e| per O• dangling bond, or a doping concentration of $\sim 10^{14}$ cm⁻².

Our estimation of doping concentration for the predominant states of graphene (weakly bound **1b–3b**) agrees with the average background charge density of 0.9×10^{12} cm⁻², which has been

estimated from a tunneling differential conductance measurement using a low-temperature scanning tunneling microscopy.⁹ The same study has also reported the amount of total charge in each puddle of the graphene ($\sim 0.3 |e|$),⁹ which is in the same ballpark as our estimation of charge transfer for **4b** ($\sim 0.24 |e|$ per O• dangling bond). Spatially resolved Raman scattering studies^{63,64} have shown that, while free-standing graphene monolayers are spatially homogeneous without intrinsic doping (with an upper bound of $\sim 10^{11} \text{ cm}^{-2}$ for the residual carrier density), supported graphenes exhibit an order of magnitude of doping variation with a few showing a high doping over $\sim 10^{13} \text{ cm}^{-2}$, which agrees with our estimation of doping concentration for **4b**.

We also propose that removing or hiding such reactive sites on SiO_2 by thermal annealing and passivation by hydrogen or organic layers (polymers or self-assembled monolayers of alkyl trimethoxysilane or hexamethyldisilazane) would reduce the charge puddle in graphene. Indeed, it has been shown^{65,66} that a graphene field-effect transistor built on a passivated SiO_2 substrate exhibits a one-order-magnitude lower carrier density than on an untreated SiO_2 substrate (supposedly with dangling bonds) but its device performance in terms of carrier mobility is doubled owing to effectively suppressed charge puddle scattering.

PDOS and Band Structure. The PDOS curves of **1b–2b** are similar to each other (Fig. 5). They are essentially the same as those of their isolated components, the bare SiO_2 surface **1–2** and the free-standing graphene. The total DOS curves of **1b–2b** are simply a sum of those of the two isolated components without any discernible perturbation to each other. The bare SiO_2 surfaces **1–2** exhibit large band gaps due to strong Si–O hybridization. The valence and conduction bands have major contributions from O and Si, respectively. Due to the large band gaps ($> 5 \text{ eV}$) of **1–2**, the binding of graphene on them (**1b–2b**) brings no new state around the Dirac point, no strong interaction between the two components, and no discernible change in PDOS. This explains the weak binding and the essential absence of charge transfer between graphene and the surfaces **1–2**. The remarkable characteristics of graphene such as the Dirac point is retained in the band structure of **1b–2b**, and the band-gap opening of graphene is negligible on both surfaces ($E_g = 5\text{--}10 \text{ meV}$; Table 3).

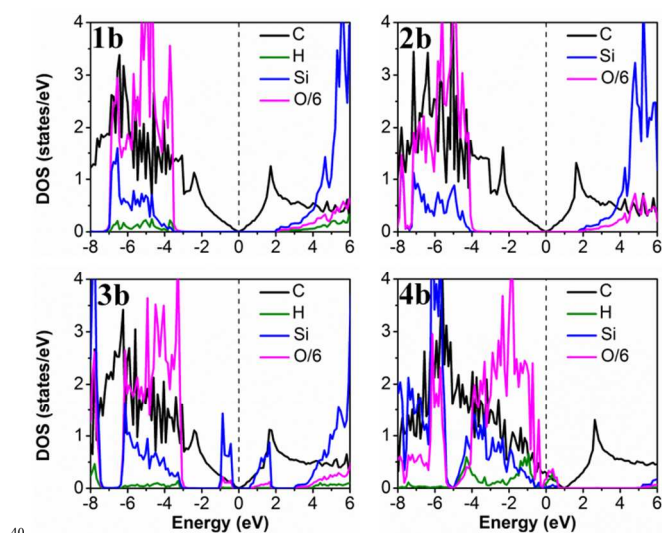


Fig. 5 DOS of **1b–4b** projected onto each element. The energy level of each system is shown relative to the Fermi energy E_F (vertical black dashed line). The PDOS for O is reduced by a factor of six for clarity.

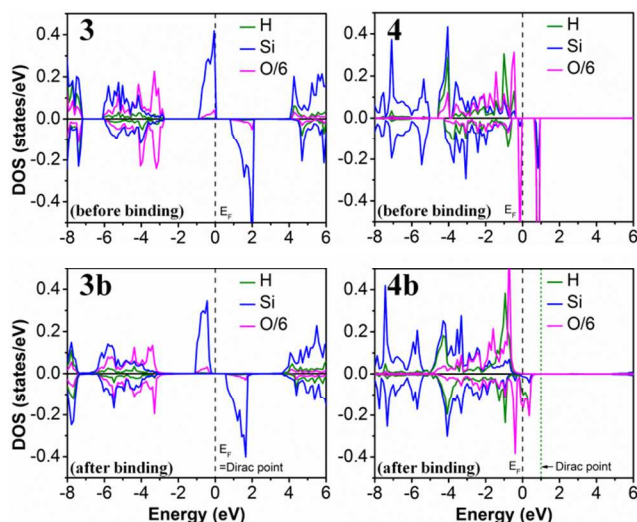


Fig. 6 Spin-polarized PDOS defined as [PDOS (spin-up) – PDOS (spin-down)] for the topmost layer of the surfaces **3–4** (upper panel) and the composites with graphene **3b–4b** (lower panel). The Dirac point of graphene (vertical green dotted line) is close to the Fermi energy E_F (vertical black dashed line at 0 eV) in the case of **3b**, but it is shifted up by 1 eV in the case of **4b**. The PDOS for O is reduced by a factor of six.

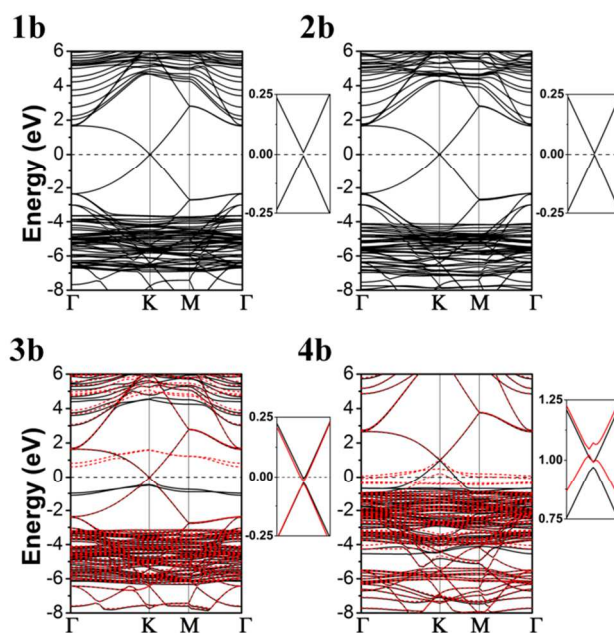


Fig. 7 Band structure of **1b–4b** with zoom-in near the Dirac point of graphene. The spin-up and spin-down components are represented by black solid and red dashed lines, respectively, for **3b–4b**. The energy level is shown relative to E_F (horizontal black dashed lines at 0 eV).

It has been reported that silicon dangling bonds on SiO_2 would significantly affect the band structure of graphene and open its band gap up to 1.2 eV .²⁸ This is not observed in our study on **3b** which has silicon dangling bonds as well. The PDOS curves of **3b** are similar to those of **1b–2b**, except for a small amount of localized Si states (two blue peaks) near the Fermi energy level E_F (vertical black dashed line) (Figs. 5–6), which originate exclusively from the defect states of the surface **3**. These defect states appear as flat bands in the middle of the large band gap ($> 5 \text{ eV}$) on each side of E_F , each of which correspond to occupied spin-up (black solid curves) and unoccupied spin-down (red

dashed curves) Si states, respectively (Fig. 7). When a surface silicon loses one of its oxygen neighbors to form a silicon dangling bond ($\bullet\text{SiOH}$), an occupied state in the Si–O hybridized valence-band region is shifted up to the mid-gap region, making the surface **3** unstable and supposedly reactive. However, this Si dangling bond ($\bullet\text{Si}$), which is located 1 Å beneath the surface hydroxyl (OH) group and tucked away from graphene, does not form a new bond with it, and thus the mid-gap defect states of **3** as well as the Dirac point of graphene are preserved intact through the binding of graphene. The DOS for **3b** is again a simple sum of those of the two isolated components without any perturbation to each other, and this is consistent with the weak binding and the negligible amount of charge transfer of graphene in **3b** as well as the negligible band-gap opening ($E_g = 17$ and 12 meV for spin-up and spin-down component, respectively; Table 3). The same trend has been observed for threefold-coordinated Si defect sites in the model surface of Rudenko and coworkers.⁶⁷

On the other hand, the PDOS curves and the band structure of **4b** exhibit a clear difference from those of **1b–3b** (Figs. 5–7). Contrary to the surface **3** whose silicon dangling bonds ($\bullet\text{SiOH}$) create the mid-gap defect states, the oxygen dangling bonds ($\text{HSiO}\bullet$) of the surface **4** create defect states right above the high-energy edge of the valence band (upper right panel, Fig. 6), and the Fermi energy of the surface **4** is brought down from the mid-gap region to this level, leaving a small amount of unoccupied state just above E_F . Contrary to the hidden silicon dangling bond ($\bullet\text{SiOH}$) of surface **3**, the oxygen dangling bond ($\text{HSiO}\bullet$) in the topmost layer of the surface **4** is exposed towards graphene, and thus a significant amount of mixing is expected between these unoccupied defect states of **4** and the occupied states of graphene. This is captured by the broadening and the partial occupation of the unoccupied defect states of **4** after binding to form **4b** (lower right panel, Fig. 6). This mixing leads to the graphene-to-SiO₂ electron transfer, that is, the *p*-doping of graphene in **4b** as well as the strong binding of graphene and the shift of the Dirac point of graphene to ~1 eV above E_F (vertical green dotted line; Figs. 5–6) in **4b**. This is consistent with the relationship between the Dirac point shift and the spatial charge inhomogeneity visualized from a differential resistance curve (dI/dV) measurement.⁷⁻⁹

The band gap of graphene in **4b** ($E_g \sim 24$ meV; Table 3) is also larger than those in **1b–3b**. (The band-gap opening of **4b** could be even larger than our estimation, considering that the PBE-D functional used in this study tends to underestimate the band gap.) In fact this is one of the largest band gaps calculated for graphene retaining the linear energy dispersion at the Dirac point. While previous calculations have reported band gaps as large as 0.1–2.9 eV for graphene on reactive SiO₂ surfaces, the band structure and the Dirac point have been completely distorted. Thus we expect that creation of a homogeneous distribution of oxygen dangling bonds ($\text{HSiO}\bullet$) on SiO₂ (001) surfaces with well-controlled O₂ plasma and partial H-passivation may lead to a band-gap opening as well as a strong binding of graphene.

4 Conclusions

Four surface models were selected to represent a variety of surface states of amorphous SiO₂ substrates and to study how these surface states affect the properties of graphene bound on them. Graphene barely bind on saturated stable surfaces (**1b–2b**) or unsaturated surfaces with silicon dangling bonds ($\bullet\text{SiOH}$; **3b**). Graphene strongly binds only on unsaturated surfaces exposing

oxygen dangling bonds ($\text{HSiO}\bullet$; **4b**). Only in this model **4b** the binding energy is close to the experimental values, implying that the presence of such reactive surface states should be responsible for the binding of graphene on SiO₂ substrates. Only in the model **4b** the adsorption of graphene leads to a significant amount of electron transfer from graphene to the surface and produces *p*-doped graphene, while the amount of charge transfer is negligible in the models **1b–3b**. This implies that the presence of reactive surface states such as **4** on amorphous SiO₂ surfaces could be one likely origin of the inhomogeneous charge distribution and the reduction of graphene mobility of supported graphenes. A better control of the surface homogeneity would therefore improve the charge transport properties of graphene for the use in electronic devices.

Acknowledgments

This work was supported by the Global Frontier Hybrid Interface Materials Program (2013M3A6B1078882), the Korean CCS 2020 Program (NRF-2013M1A8A1040838), and the Basic Research Program (NRF-2013R1A1A3012254) of the National Research Foundation of Korea funded by the Ministry of Science, ICT & Future Planning. This work was also supported by the Brain Pool Program (121S-1-3-0380 and 131S-1-3-0504) of KOFST, the Inter-ER Cooperation Project (R0000499) of KIAT/MKE, the Grand Challenge Program (KSC-2012-C2-12) and the PLSI supercomputing resources of KISTI, and also by GIST Specialized Research Project of GIST.

Notes and references

- ^a School of Materials Science and Engineering, Gwangju Institute of Science and Technology, Gwangju 500-712, Korea (yhjang@gist.ac.kr)
- ^b GREMAN, UMR 7347, Université François Rabelais, Tours 37200, France (lansac@univ-tours.fr)
1. K. S. Novoselov, A. K. Geim, S. V. Morozov, D. Jiang, Y. Zhang, S. V. Dubonos, I. V. Grigorieva and A. A. Firsov, *Science*, 2004, **306**, 666-669.
2. A. K. Geim and K. S. Novoselov, *Nat. Mater.*, 2007, **6**, 183-191.
3. F. Schwierz, *Nat. Nanotechnol.*, 2010, **5**, 487-496.
4. K. S. Novoselov, A. K. Geim, S. V. Morozov, D. Jiang, M. I. Katsnelson, I. V. Grigorieva, S. V. Dubonos and A. A. Firsov, *Nature*, 2005, **438**, 197-200.
5. A. H. Castro Neto, F. Guinea, N. M. R. Peres, K. S. Novoselov and A. K. Geim, *Rev. Mod. Phys.*, 2009, **81**, 109-162.
6. S. V. Morozov, K. S. Novoselov, M. I. Katsnelson, F. Schedin, D. C. Elias, J. A. Jaszczak and A. K. Geim, *Phys. Rev. Lett.*, 2008, **100**, 016602.
7. J. Martin, N. Akerman, G. Ulbricht, T. Lohmann, J. H. Smet, K. v. Klitzing and A. Yacoby, *Nat. Phys.*, 2007, **4**, 144-148.
8. A. Deshpande, W. Bao, F. Miao, C. N. Lau and B. J. Leroy, *Phys. Rev. B*, 2009, **79**, 205411.
9. Y. Zhang, V. W. Brar, C. Girit, A. Zettl and M. F. Crommie, *Nat. Phys.*, 2009, **5**, 722-726.
10. A. Deshpande, W. Bao, Z. Zhao, C. N. Lau and B. J. LeRoy, *Phys. Rev. B*, 2011, **83**, 155409.
11. E. H. Hwang, S. Adam and S. Das Sarma, *Phys. Rev. Lett.*, 2007, **98**, 186806.
12. Y. A. Eva, L. Guohong and D. Xu, *Rep. Prog. Phys.*, 2012, **75**, 056501.
13. J. C. Meyer, A. K. Geim, M. I. Katsnelson, K. S. Novoselov, T. J. Booth and S. Roth, *Nature*, 2007, **446**, 60-63.
14. A. Fasolino, J. H. Los and M. I. Katsnelson, *Nat. Mater.*, 2007, **6**, 858-861.
15. M. Gibertini, A. Tomadin, F. Guinea, M. I. Katsnelson and M. Polini, *Phys. Rev. B*, 2012, **85**, 201405.

16. M. Ishigami, J. H. Chen, W. G. Cullen, M. S. Fuhrer and E. D. Williams, *Nano Lett.*, 2007, **7**, 1643-1648.
17. C. H. Lui, L. Liu, K. F. Mak, G. W. Flynn and T. F. Heinz, *Nature*, 2009, **462**, 339-341.
18. W. G. Cullen, M. Yamamoto, K. M. Burson, J. H. Chen, C. Jang, L. Li, M. S. Fuhrer and E. D. Williams, *Phys. Rev. Lett.*, 2010, **105**, 215504.
19. J. H. Chen, C. Jang, S. Adam, M. S. Fuhrer, E. D. Williams and M. Ishigami, *Nat. Phys.*, 2008, **4**, 377-381.
20. A. Castellanos-Gomez, R. H. M. Smit, N. Agrait and G. Rubio-Bollinger, *Carbon*, 2012, **50**, 932-938.
21. K. M. Burson, W. G. Cullen, S. Adam, C. R. Dean, K. Watanabe, T. Taniguchi, P. Kim and M. S. Fuhrer, *Nano Lett.*, 2013, **13**, 3576-3580.
22. P. Joshi, H. E. Romero, A. T. Neal, V. K. Toutam and S. A. Tadigadapa, *J. Phys.: Condens. Matter*, 2010, **22**, 334214.
23. H. E. Romero, N. Shen, P. Joshi, H. R. Gutierrez, S. A. Tadigadapa, J. O. Sofo and P. C. Eklund, *ACS Nano*, 2008, **2**, 2037-2044.
24. T. P. M. Goumans, A. Wander, W. A. Brown and C. R. A. Catlow, *Phys. Chem. Chem. Phys.*, 2007, **9**, 2146-2152.
25. W. Steurer, A. Apfelter, M. Koch, T. Sarlat, E. Søndergård, W. E. Ernst and B. Holst, *Surf. Sci.*, 2007, **601**, 4407-4411.
26. E. Papirer, Balard, H., *The Surface Properties of Silicas*, edited by A. P. Legrand, Wiley, New York, 1998.
27. F. Bart and M. Gautier, *Surf. Sci.*, 1994, **311**, L671-L676.
28. Y. J. Kang, J. Kang and K. J. Chang, *Phys. Rev. B*, 2008, **78**, 115404.
29. M. Z. Hossain, *Appl. Phys. Lett.*, 2009, **95**, 143125.
30. P. Shemella and S. K. Nayak, *Appl. Phys. Lett.*, 2009, **94**, 032101.
31. T. C. Nguyen, M. Otani and S. Okada, *Phys. Rev. Lett.*, 2011, **106**, 106801.
32. K. Chen, X. Wang, J. B. Xu, L. Pan and Y. Shi, *J. Phys. Chem. C*, 2012, **116**, 6259-6267.
33. P. Havu, M. Ijäs and A. Harju, *Phys. Rev. B*, 2011, **84**, 205423.
34. X. F. Fan, W. T. Zheng, V. Chihaiia, Z. X. Shen and J. L. Kuo, *J. Phys.: Condens. Matter*, 2012, **24**, 305004.
35. F. Messina and M. Cannas, *J. Phys. Chem. C*, 2007, **111**, 6663-6667.
36. L. Levien, C. T. Prewitt and D. J. Weidner, *Am. Mineral.*, 1980, **65**, 920-930.
37. P. Trucano and R. Chen, *Nature*, 1975, **258**, 136-137.
38. G. Kresse and J. Furthmüller, *Phys. Rev. B*, 1996, **54**, 11169-11186.
39. S. Grimme, *J. Comput. Chem.*, 2004, **25**, 1463-1473.
40. S. Grimme, *J. Comput. Chem.*, 2006, **27**, 1787-1799.
41. J. P. Perdew, K. Burke and M. Ernzerhof, *Phys. Rev. Lett.*, 1996, **77**, 3865-3868.
42. J. P. Perdew, K. Burke and M. Ernzerhof, *Phys. Rev. Lett.*, 1997, **78**, 1396-1396.
43. G. Mercurio, E. R. McNellis, I. Martin, S. Hagen, F. Leyssner, S. Soubatch, J. Meyer, M. Wolf, P. Tegeder, F. S. Tautz and K. Reuter, *Phys. Rev. Lett.*, 2010, **104**, 036102.
44. A. Otero-De-La-Roza and E. R. Johnson, *J. Chem. Phys.*, 2012, **137**, 054103.
45. P. E. Blöchl, *Phys. Rev. B*, 1994, **50**, 17953-17979.
46. G. Kresse and D. Joubert, *Phys. Rev. B*, 1999, **59**, 1758-1775.
47. H. J. Monkhorst and J. D. Pack, *Phys. Rev. B*, 1976, **13**, 5188-5192.
48. P. E. Blöchl, O. Jepsen and O. K. Andersen, *Phys. Rev. B*, 1994, **49**, 16223-16233.
49. R. F. W. Bader, *Atoms in Molecules: A Quantum Theory* Oxford University Press, New York, 1994.
50. G. Henkelman, A. Arnaldsson and H. Jónsson, *Comput. Mater. Sci.*, 2006, **36**, 354-360.
51. W. Tang, E. Sanville and G. Henkelman, *J. Phys.: Condens. Matter*, 2009, **21**, 084204.
52. K. Momma and F. Izumi, *J. Appl. Crystallogr.*, 2011, **44**, 1272-1276.
53. N. H. De Leeuw, F. M. Higgins and S. C. Parker, *J. Phys. Chem. B*, 1999, **103**, 1270-1277.
54. D. R. Lide, *CRC Handbook of Chemistry and Physics*, 87th edn., CRC Press, Boca Raton, 2006-2007.
55. M. F. Yu, T. Kowalewski and R. S. Ruoff, *Phys. Rev. Lett.*, 2001, **86**, 87-90.
56. P. Staszczuk, B. Jańczuk and E. Chibowski, *Mater. Chem. Phys.*, 1985, **12**, 469-481.
57. G. M. Rignanese, A. De Vita, J. C. Charlier, X. Gonze and R. Car, *Phys. Rev. B*, 2000, **61**, 13250-13255.
58. C. F. Abrams and D. B. Graves, *J. Vac. Sci. Technol. A*, 1998, **16**, 3006-3019.
59. J. Henri, G. Han, B. Meint de, E. Miko and F. Jan, *J. Micromech. Microeng.*, 1996, **6**, 14.
60. S. P. Koenig, N. G. Boddeti, M. L. Dunn and J. S. Bunch, *Nat. Nanotechnol.*, 2011, **6**, 543-546.
61. J. N. Israelachvili, *Intermolecular and Surface Forces*, 3rd edn., Academic Press, New York, 2011.
62. X. Liang, Z. Fu and S. Y. Chou, *Nano Lett.*, 2007, **7**, 3840-3844.
63. S. Berciaud, S. Ryu, L. E. Brus and T. F. Heinz, *Nano Lett.*, 2009, **9**, 346-352.
64. C. Casiraghi, S. Pisana, K. S. Novoselov, A. K. Geim and A. C. Ferrari, *Appl. Phys. Lett.*, 2007, **91**, 233108.
65. K. Chen, X. Wan, D. Liu, Z. Kang, W. Xie, J. Chen, Q. Miao and J. Xu, *Nanoscale*, 2013, **5**, 5784-5793.
66. S.-Y. Chen, P.-H. Ho, R.-J. Shiu, C.-W. Chen and W.-H. Wang, *Nano Lett.*, 2012, **12**, 964-969.
67. A. N. Rudenko, F. J. Keil, M. I. Katsnelson and A. I. Lichtenstein, *Phys. Rev. B*, 2011, **84**, 085438.